Structural evaluation of ultralight solar sails and sunshades under different load conditions

SIMON STENBERG

Structural evaluation of ultralight solar sails and sunshades under different load conditions

Simon Stenberg, *MSc student, KTH, Royal Institute of Technology, Stockholm, Sweden*

Abstract—Solar sails are an innovative propulsion mechanism for space exploration, harnessing the momentum of photons from the Sun to propel spacecraft. As material science advances and launch costs continue to fall, opportunities utilising the novel characteristics of solar sails become more and more feasible. Due to the inherit connection between mass and acceleration, it is of great importance to reduce mass to gain acceleration. This thesis investigates the structure of solar sails and provides an analysis of the forces they encounter. The study examines the forces acting on circular solar sails in space, as well as the unique challenges they face on Earth and during the launch phase. The membrane and supporting composite structure is analysed using mathematical models in MATLAB in order to develop and optimize structures for strength and reduced mass. Dimensioning forces were found and a preliminary structure discussed. By understanding these forces, it is possible to optimize the design and deployment of solar sails, paving the way for more efficient space missions.

Index Terms—Solar sailing, solid mechanics, membrane, composites

Sammanfattning—Solsegel är en innovativ framdrivningsmekanism för rymdforskning som utnyttjar fotoners rörelsemängd från solen fotoner för att driva rymdfarkoster. I takt med att materialvetenskapen utvecklas och uppskjutningskostnader fortsätter att sjunka, blir möjligheterna att använda solsegels unika egenskaper alltmer genomförbara. På grund av det naturliga sambandet mellan massa och acceleration är det av stor vikt att minska massan för att öka accelerationen. Detta examensarbete undersöker strukturen hos solsegel och ger en analys av de krafter de utsätts för i olika stadier under dess livscykel. Studien granskar de krafter som verkar på seglen i rymden, samt de unika utmaningar de står inför på jorden och under uppskjutningsfasen. Membranet och den stödjande kompositstrukturen analyseras med hjälp av modeller i MATLAB för att utveckla och optimera strukturer med avseende på styrka och vikt. Genom att förstå dessa krafter är det möjligt att optimera utformningen och utplaceringen av solsegel, vilket banar väg för allt mer effektiva och unika rymduppdrag.

NOMENCLATURE

Acronyms

AU   Astronomical Unit
CFRP   Carbon-fiber-reinforced polymers
COG   Center of gravity
ECSS   European Cooperation for Space Standardization
ESA   European Space Agency
FEM   Finite Elements Method
HF   High-Frequency
Hz   Hertz
IKAROS Interplanetary Kite-craft Accelerated by Radiation Of the Sun
JAXA   Japanese Aerospace Exploration Agency
JPL   Jet Propulsion Laboratory
KTH   Royal Institute of Technology
LEO   Low Earth Orbit
LF   Low-Frequency
NASA   National Aeronautics and Space Administration
QSL   Quasi-static load
SLS   Space Launch System
STD   Standard
TRL   Technology Readiness Level

CONTENTS

I. INTRODUCTION

SOLAR sails are a propulsion method relying on radiation pressure from a light source to generate its acceleration. Unlike the common chemical and electrical systems found in typical spacecraft, this method expends no fuel, instead harnessing the momentum of photons. An analogy often made is that of a sail boat; as the wind acts on the sails of a boat propelling it forward, the photons act on the spacecraft, accelerating it. The pressure is typically small, which constrains solar sails to have large areas and low structural and payload mass. Solar sails are a departure from conventional propulsion methods, offering unique benefits and drawbacks, with the largest advantage being the elimination of an onboard propulsion system and fuel. Given a suitable light source, this could provide unlimited propulsion [1].

Einstein's relativistic equation in regards to the mass-energy equivalence can be formulated as

$$E^2 = (m_0 c^2)^2 + (pc)^2 \tag{1}$$

where E is the relativistic energy, m_0 is an object's rest mass, p is its momentum, and c is the speed of light. It is in the exchange of momentum from the photons to the sail which propels the spacecraft forward. Where each photon has the momentum

$$p = h\lambda \tag{2}$$

and the total pressure

$$P = \frac{F}{A} = \frac{W}{c}. \tag{3}$$

The total radiative power of the Sun is approximately 3.84×10^{26} W [2] and the amount of radiation per unit area, flux, at distance r_s away from the Sun can be expressed as

$$W(r_s) = \frac{L_\circ}{4\pi r_s^2}. \tag{4}$$

As can be seen in Eq. (4), the inverse square law leads to a drastic decrease in solar flux when the distance increases, as illustrated by Fig. 1. This fundamental aspect of solar sailing constrains missions as the force decreases. A lightness number β is often introduced, a property of the Sun and the spacecraft mass, independent from the distance r_s[3]. It is a function of the loading on the sail, σ, and a constant from the sun which can be written as
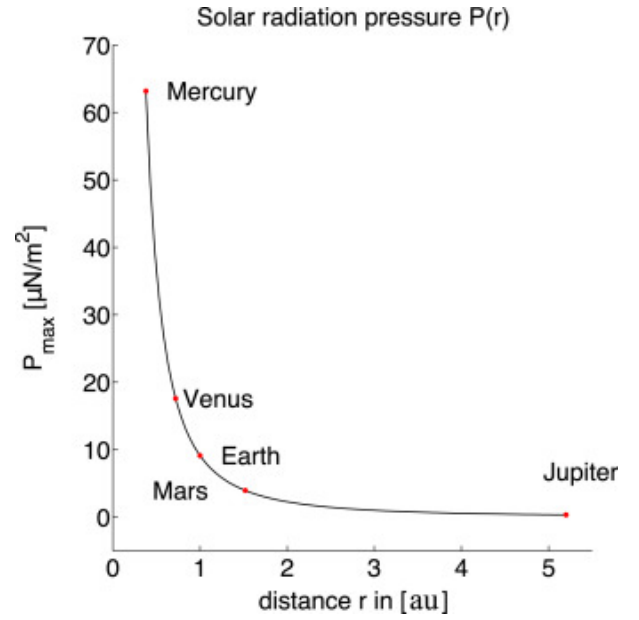

Fig. 1. Solar radiation pressure as a function of radius

$$\beta = \frac{\sigma^*}{\sigma} \tag{5}$$

where

$$\sigma = m/A \tag{6}$$

and σ^* the solar constant of 1.53 g/m^2. The parameter is a useful indicator of solar sail performance and acceleration as a higher lightness number lowers the sail loading, increasing acceleration. This can be achieved either by reducing mass or using a larger sail. Modern sail technology has a lightness number of between $\beta = 0.01 - 0.03$. Near term advancements in sail material currently at a low TRL could produce lightness numbers of 0.05 [4].

There are a multitude of factors that go in to calculating the force on the solar sail, many of these relate to the material used for the sail. These include absorption, transmission, reflection and other optical properties [5]. In this report however, a simplified and idealized model is used and can be visualized in Fig. 2 with the force and acceleration expressed as

$$\mathbf{F} = 2P(r)A\cos^2(\theta)\mathbf{n} \tag{7}$$

and

$$a_s = \frac{2PA_s}{m_s}\cos^2\theta \tag{8}$$

where $P(r)$ is solar pressure at radius r, θ the angle between the sail normal $\mathbf{n}$ and the position vectors [6]. The force F is small for any reasonable size of sail. At 1 AU the pressure from solar radiation is ca 4.5×10^{-6} N/m^2. To put that into perspective, a force of 1 N would require a square sail with a side of 470 m.
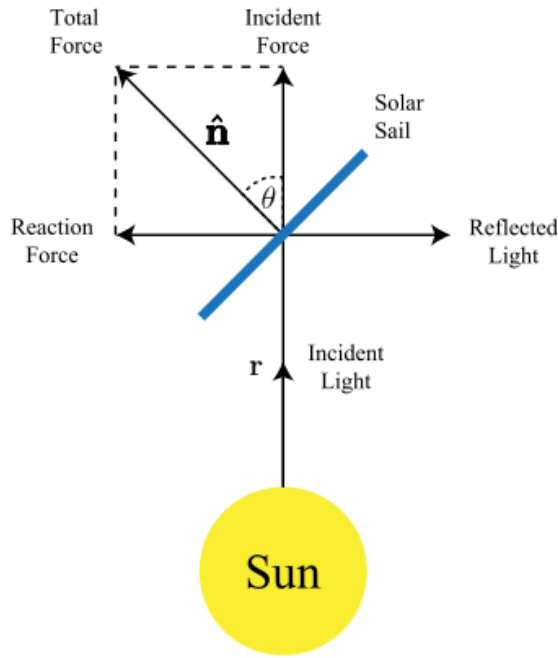
Fig. 2. Sun-Sail interaction

A. History

1) Early developments: In the mid 19th century, James Clerk Maxwell published his theories on electromagnetism showing that light had momentum and exerted a pressure. This laid the fundamental groundwork for the physics behind solar sailing. However, it was in the early 20th century that the first scientific papers on the subject of solar spacecraft were published. Carl Sagan popularised the idea in the early 1970s and the first formal design and technological endeavours started at NASA in 1976. Solar pressure acts on all bodies in space and is corrected for in most spacecraft. A typical spacecraft trajectory to Mars would be pushed thousands of kilometers off course if not corrected. Spacecraft such as the Mariner 10 and Hayabusa mission used solar pressure as attitude control to conserve fuel and compensate for broken components, respectively. The first deployment of a solar sail like structure in space was the Russian Znamya-2 mission launched in 1992 [7]. The goal was to test the deployment and function of a circular solar reflector and to beam sunlight back to Earth. The mission was seen as a success and demonstrated the feasibility and control of a deployable, lightweight, sun reflector.

2) Previous spacecraft: The first spacecraft using solar pressure as the primary means of propulsion was the IKAROS spacecraft developed by the Japanese space agency (JAXA) in 2010. IKAROS was a technology demonstrator with a 14×14 m^2 sail and gained 100 m/s over a six month period. IKAROS marks a significant development in application of solar sails. Also in 2010, Nanosail-D launched with the goal of testing the passive de-orbiting potential of solar sails, by increasing solar and atmospheric drag. Nanosail-D showed the potential of solar sails in sustainability efforts to reduce space debris.

3) Future developments: Looking ahead, NASA's Solar Cruiser project slated to launch in early 2025 was the largest solar sail in physical development. However, due to budgetary constraints the mission was canceled and only a quarter of it's original sail will be launched as a technology test bed. Solar cruiser's sail would have been 1670 m^2 marking a significant leap in solar sail size over previous missions. The aim was to insert the Solar Cruiser into a novel heliocentric polar orbit kept in place by solar pressure. It was proposed to maintain a position sunward of the Lagrange point L1, a location where Earth's and the Sun's gravity balance with the centripetal force along the Sun-Earth line, and study the space weathers effect on the heliosphere. Greschik [8] proposed a system of circular solar sails connected together, much like a dog sled, to tow a payload behind it. By dividing the sail area over multiple panels, Greschik found that even with conservative estimates, relatively large payloads could be flown and at a lower cost compared to traditional solar sails. Greschik's proposal did not receive much interest. Moreover, a research project called Starshot [9] has proposed using lasers to impart a large amount of power on a solar sail for a moment, accelerating it up to fractions of the speed of light. This project aims to send small solar sails to Alpha Centaruri, 4.4 light years away. An enormous phased laser array would aim at solar sails in LEO and impart up to 100 GW. At the moment, the feasibility of the mission is low due to technical and budgetary limitations, but shows further applications of solar sailing in the future.

B. Benefits and Drawbacks

The main challenges with solar sails relate to the small force and slow acceleration. Missions are long duration in nature as achieving any significant velocity increase using solar sails takes a considerable amount of time. Therefore solar sail technology does not lend itself to short duration missions or missions requiring rapid velocity changes such as docking, orbital insertions, etc. A downstream effect of the small forces involved is the large significance of spacecraft mass. As the spacecraft acceleration is given by Newton's second law, $F = ma$, the mass is directly proportional to its acceleration. It is therefore of utmost importance to reduce overall spacecraft mass as to maximise acceleration. This also limits the amount of allowable payload mass that the spacecraft can carry. A solution is to increase the sail volume and thus get more acceleration. However, increasing area while minimizing mass has stretched current material technology to its limits, with the upcoming NASA solar cruiser having an area of 40×14 m^2. Anything larger than this would most likely need more advancements in material science.

Sail material has seen a development in the 21st century. Advancements have been made in regards to properties as reflection and absorption as well as reduced thickness, reducing sail mass and increasing force per unit area. With long duration missions the long term durability of sail material is also critical. Many outside factors can damage the sail material, such as electron radiation or cosmic dust effecting optical properties and space debris piercing the sail [10]. The reduction in efficiency from sail degradation is further compounded by the reduced solar radiation as the distance from the

Sun increases. This further reduces the solar sail's acceleration and limits the possible missions utilizing solar sails as primary propulsion. A further effect of small acceleration is the relative size of disturbance forces being larger and thus having a larger effect on the spacecraft trajectory [11]. Disturbances that can potentially be found in a space environment and their sources can be seen in Tab I. These disturbances need to be modeled accurately due to the relatively large effect they have on the sail in contrast with traditional spacecraft.

TABLE I
DISTURBANCE FORCES ON A TYPICAL SOLAR SAIL

Disturbance Force	Source
Solar radiation pressure	Solar pressure from the Sun
Gravity gradient	Off-diagonal inertia of the spacecraft causes body fixed torque
Gravitational potential	Shape of non-spherical nearby body
Third body perturbation	Gravitational effect of large bodies
Residual dipole	Internal currents may create a dipole which interacts with the magnetic field causing torque
Aerodynamic drag	Atmosphere of nearby body
Albedo pressure	Sun reflection from nearby body
Outgasing	Trapped humidity in structure
Radiation pressure	Heat from nearby body generating force on spacecraft
Radio transmissions	Communication equipment producing RF pressure during transmission
Thermal pressure	Radiators, heat sources diffusing
Leaks	Onboard gas and liquid storage
Thruster plumes	Thruster system may expel plumes effecting spacecraft trajectory

The main benefit to solar sails is the elimination of an onboard propulsion system. With an unlimited propulsion source being supplied from the Sun, missions previously unfeasible using chemical and electric propulsion may be in the realm of possibility. Mission examples include traveling to the inner planets and using a solar sail, unfurling it and passively return and retrieve samples back to Earth [2]. Orbits which may not be stable could employ solar sails to balance out forces. Furthermore, thanks to the lack of onboard propulsion, mission life could be extended using solar sails. A satellite in low Earth orbit could utilise solar pressure for station keeping and maintain a desired orbit whilst a conventional satellite would de-orbit [3]. As launch cadence increases year by year, more and more space debris litters orbits, several plans have been put forth to deploy a solar sail and utilize solar pressure and atmospheric drag to de-orbit satellites at their end of life [7]. As the amount of space debris increases, solar sails my offer a viable prevention. Lastly, due to the relative simplicity of solar sails in contrast to chemical or electrical propulsion, spacecraft utilizing solar sails may be several times cheaper which could further benefit the technology.

C. Types of sails

In literature, four main types of solar sail configurations are often discussed. Their simplified geometries can be seen in Fig 3. These include the square, circular, spinning disk and heliogyro. They all use the same mechanics of propulsion but go about it in unique ways for optimal performance depending on the mission criteria.
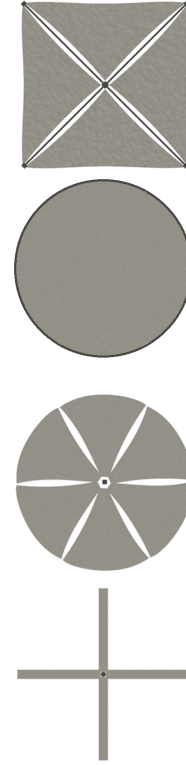

Fig. 3.   Common solar sail configurations [12]

1) Square sails: The square sail is the most common type, as evidenced by previous missions. It usually consists of four deployable booms, also called masts, which support the sail membrane. Square sails typically has the highest force due to the large surface area in contrast with other types. The membrane can be pulled taught which minimizes hot spots and fluttering of the sail. Some issues can arise with the deployment of the booms and sail, which has been seen in some missions. These include ripping of the sail membrane [13] as well as problems with the boom unfurlment [8]. Overall, square sails provide good force to mass ratios and are relatively scalable, up to certain sizes.

2) Circular sails: Circular sails are the most simple of the four. In its most basic configuration, it consists of an outer ring supporting a circular membrane strung within. There are several different types of ring structures, they can be a solid structure such as a carbon fiber composite or a deployable structure utilising inflation or even magnetic fields [14]. Proposals have been put forwards by Greschik [8] to use a large number of simple disk sails to tow a payload behind it. By towing, issues such as bending moments on large solar sail beams are negated whilst retaining large surface areas [8].

3) Spinning Disk: The spinning disk sail was developed by JPL in the 1970s. By spinning the sail, the spacecraft uses centrifugal force to passively deploy and subsequently apply tension to the sail. The spinning has the added benefit of spacecraft stability compared to its non rotating counterparts. The sail is often times segmented up to reduce wrinkles on the sail surface, connected with gores that flex due to the

centrifugal force pulling the panels tight [15].

4) Heliogyro: Much like the spinning disk, the heliogyro was conceived by JPL and uses spin to provide tension and deploy the spacecraft. The heliogyro derives its name from helio, the sun, and gyro, spinning. It uses helicopter-like blades attached to a central structure which can gimbal to change rotation and attitude. Similar to the spinning disk, the heliogyro has the benefit of simple deployment. The surface area of the spacecraft is however very small and requires many, long, blades to produce meaningful force [15].

II. PROBLEM

Mass reduction has always been a cornerstone of spaceflight and solar sails are no exception. Due to the extremely low force, reducing mass is of great importance. This thesis aims to analyse the forces solar sails are subjected to and provide a holistic understanding on limiting factors. These factors include excessive sagging and stress of the sail membrane and buckling and of the supporting structure. A circular sail with a supporting torus and membrane will be considered. Forces such as gravity, transportation and handling as well as solar radiation pressure being investigated. A simple and lightweight structure is sought after, much like the ones proposed by Greschik [8] for the space tow system. The toroid would be as large as possible, as to maximaise area, given fairing limitations (8 m diameter) on launchers such as the Ariane 5, SLS and Starship. Furthermore, it is assumed that the sail material is limited to current technology and product offerings.

III. METHOD

A. Circular sail membrane

A circular sail supported at its perimeter, can be modelled as a circular isotropic elastic membrane. Hencky's problem [16] analyses initially flat membranes with a circular boundary subjected to a lateral load [17]. Using this approach the stress and lateral displacement, Δh, of the sail can be examined. Two main problems arise when applying Hencky's problem. The first of which is an algebraic error in his original 1915 paper [18]. The second, is that Hencky's solution involves a strictly lateral uniform load. Therefore, the radial component, which is of significance as the deflection increases, is neglected. These issues are handled by using a corrected version of Hencky's problem and assuming displacements of $\Delta h/D < 0.02$. At these deflections, the error term is small and will be compared with other displacement methods in upcoming chapters. Fichter [19] found that this method agrees quite closely for small load cases but will diverge as the load is increased. The displacement limit criterion of displacements of $\Delta h/D < 0.02$ was was chosen due to the geometric problems which may arise as a result of the sagging. Moreover, it was estimated that around this displacement the material stress would start to be of issue as well. The problem needs to fulfill the following criteria, namely

- Uniform thickness
- Circular isotropic elastic membrane
- Clamped at boundary

- No pre-tension
- Uniform lateral load.

Fichter [19] covers the derivation for both Hencky's problem as well as his own uniform pressure solution in great detail. In this thesis a shorter summary is presented, for a comprehensive explanation, see [19]. The governing radial and lateral equations are

$$N_\theta = \frac{\mathrm{d}}{\mathrm{d}r}\left(r_m N_r\right) \tag{9}$$

$$N_r \frac{\mathrm{d}w}{\mathrm{d}r} = -\frac{p_m r_m}{2} \tag{10}$$

where N_θ and N_r are tangential and radial stress resultants, r_m the radial membrane coordinate, w the lateral deflection and p_m our load. From this point the stresses can be derived as

$$N_\theta = \frac{E_m t_m}{4} q^{\frac{2}{3}} \sum_{n=0}^{\infty} b_{2n} \rho^{2n} \tag{11}$$

$$N_r = \frac{E_m t_m}{4} q^{\frac{2}{3}} \sum_{n=0}^{\infty} (2n+1) b_{2n} \rho^{2n}. \tag{12}$$

with

$$\rho = \frac{r_m}{R_m} \quad , \quad q = \frac{p_m R_m}{Et} \tag{13}$$

and

$$N = \frac{N_r}{E_m h_m} \quad , \quad W_m = \frac{w}{R_m} \tag{14}$$

The stress and deflection is then expressed as a function of the radial coordinate r_m and find

$$N(\rho) = \frac{1}{4} q^{\frac{2}{3}} \sum_{n=0}^{\infty} b_{2n} \rho^{2n} \tag{15}$$

$$W(\rho) = q^{\frac{1}{3}} \sum_{n=0}^{\infty} a_{2n} (1 - \rho^{2n+2}). \tag{16}$$

The factors b_{2n} and a_{2n} are power series solutions found using the boundary condition $W(r_m) = u(R_m) = 0$. These solutions can been seen in [19] . Both terms are expressed in terms of b_0, which in turn depends on Poisson's ratio, μ. The values of b_0 as a function of μ for $\mu_{0.2}$, $\mu_{0.3}$, $\mu_{0.4}$ gives the values of b_0 as $1.6827, 1.7244, 1.7769$.

At this point, and when the loads are known, a MATLAB code can be created which can solve Hencky's problem. From this code, the strain, deflection and the deformed shape can be found, as well as solving for different loads given boundaries on material thickness and applied force.
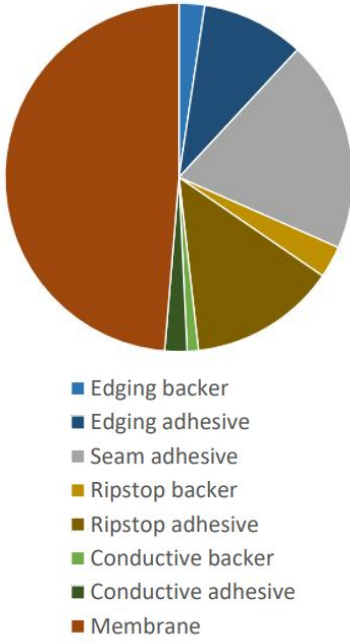
Fig. 4.   Mass distribution of sail membrane

Fig. 5.   Toroid-membrane construction (not to scale)

B. Membrane material

While sail membranes are often seen as uniform materials[20], they consist of many different materials [21]. The materials can be grouped in three categories; membrane, adhesive and rip stop. Depending on the construction, the membrane material may only make up half of the total sail mass [22]. As seen in Fig.4, adhesive makes up a large amount of residual mass. It is due to this distribution, assumed that the final sail mass will assumed to be twice that of the membrane material mass. In construction, rolls of membrane material are laid out and adhered using adhesive. Rip stop cord is then placed perpendicular to the seams. Rip stop is often constructed out of Kevlar and acts to stop potential rips in the membrane from propagating. The membrane, which typically makes up the majority of the volume, is in turn made up of several layers. The thickest layer, around $2-5$ μm, consists of a polymer material, often Mylar, Kapton or Teonex [23]. Of which Kapton was chosen for this report due to its good strength and the vast amount of material data available. On the sun side, using vapor deposition, a thin 100 nm film of aluminium is added to give the reflective properties. On the dark side, an approx 15 nm coating of black chromium is sometimes added to increase emissivity to manage temperature. The mechanical properties for Kapton that are needed for the analysis are

- Young's modulus, E_m, 2.5 GPa
- Tensile strength, σ_y, 87 MPa
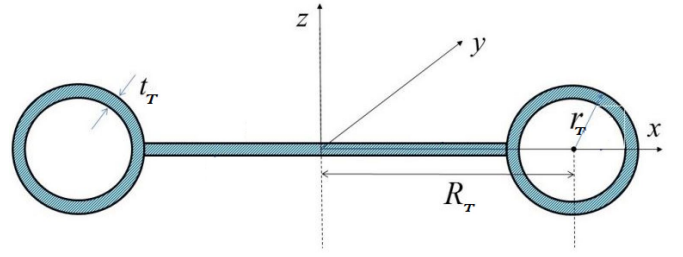- Density, 1420 kg/m^3
- Poisson's ratio, υ, 0.3 [24].

C. Toroidal ring

For this thesis, a carbon-composite toroidal ring will be investigated. The ring's radius R_T and r_T are it's radius and shell radius and t_T the cross sectional thickness (Fig. 5). It is assumed that $r_T \ll R_T$ and that $t_T \ll r_T$ which dictates that membrane theory can be used [14]. The force exerted from the solar pressure acts upon the sail, which in turn is supported by the structure. In the case of a circular toroid this resulting load will be equal and act upon the perimeter of the toroid. Studies have found that the direction of a load has a large effect on the buckling load [25]. It is in the case of the chosen sail membrane assumed that there will be small deformations resulting in small angles changes and thus a constant direction load. When the toroid is subjected to a load it may buckle due to both in plane and out-of-plane simultaneously. As the ring has an axis of symmetry these two phenomenon are uncoupled and can be investigated separately. Many different analysis and approaches have tackled this problem, with varying methods and accuracy. Weeks [26] covers his findings in using the energy method. The governing equation is

$$\delta\Pi_1 + \delta\Pi_2 + \delta\Pi_3 - \delta W = 0 \tag{17}$$

where Π_1 is strain energy, Π_2 potential energy due to internal pressure, Π_3 potential energy of the pre-buckling stress membrane acting through the buckling strain, and W the work done. Weeks [26] studied an inflatable toroid but the pressure term can be ignored for a non-pressurised structure. By calculating energies and looking at the lowest buckling mode $(n = 2)$ Weeks found that the buckling of a toroid can be expressed as

$$q_{cr} = \gamma \frac{E_T I_T}{R_T^3} \tag{18}$$

where I_t is the second moment of area for a toroid $I = \pi r^3 t$ and γ is a load parameter depending on the type of buckling, either in-plane, or out-of-plane. For in-plane loading, this loading parameter is expressed as

$$\gamma_{IP} = \frac{4}{1 + \frac{2}{3}k + \frac{4(1+k)}{S} + \frac{1+2k}{T}} \tag{19}$$

and the out-of-plane

$$\gamma_{OOP} = \frac{\frac{9+1.125\Gamma}{S}}{4 + 5k + \frac{1+5k}{\Gamma} + \frac{12.375+13.875k}{S} + \frac{\Gamma}{S}(0.5 + 0.625k)} \tag{20}$$

where

$$S = \frac{A_T G_T R_T^2}{2 E_T I_T}, \qquad T = \frac{E_T A_T R_T^2}{E_T I_T}, \qquad \Gamma = \frac{J_T G_T}{E_T I_T} \tag{21}$$

and

$$k = \frac{r_T}{R_T}, \qquad J = 2\pi r_T^3 t_T. \tag{22}$$

If the shear stiffness, S, goes towards infinity and it is assumed that $r_T \ll R_T$ Eqs. (19) and (20) can be simplified to get

$$\gamma_{IP} = 4 \tag{23}$$

and

$$\gamma_{OOP} = \frac{9}{4 + \frac{1}{\Gamma}}. \tag{24}$$

It can be observed that for most cases the out-of-plane buckling load will be the smallest and therefore limiting factor for the toroid. Finally, Eqs. (23) and (24) can be substituted into (18) to find the critical buckling load for the structure [27]. The following inequality can now be introduced for our maximum load without buckling as

$$q_{\text{cr}} \leq \gamma_{\text{cr}} q \tag{25}$$

where q_T is the force from the membrane transmitted to the torus, where the force is found by projecting the membrane stress onto the torus plane and is simply expressed as

$$q_T = \frac{m_M a}{R_T} \tag{26}$$

with m_M the membrane mass and a being the acceleration at different stages of the membranes life cycle, such as lift-off, handling and Earth's gravity, and will be touched upon further on.

D. Bending of cantilevered toroid

A specific problem which could occur is buckling or material failure of the ring during handling on the ground. If the ring were to be picked up on two opposite sides a moment arm occurs as the center of gravity of each semicircle, with the mass of the toroid and membrane structure acting upon it. Buckling of composites is a complex issue. There are many failure modes and many factors affecting the strength. The strength of carbon fiber is in large part dictated by the material itself but also who the fibers are oriented relative to the structure and the forces acting upon it. It is possible to tailor the structure to the loads to optimise for strength and mass [28]. This endeavour necessitates a good understanding of all forces involved and rigorous FEM analysis. For this, thesis a typical strength carbon composite, with isotropic properties is
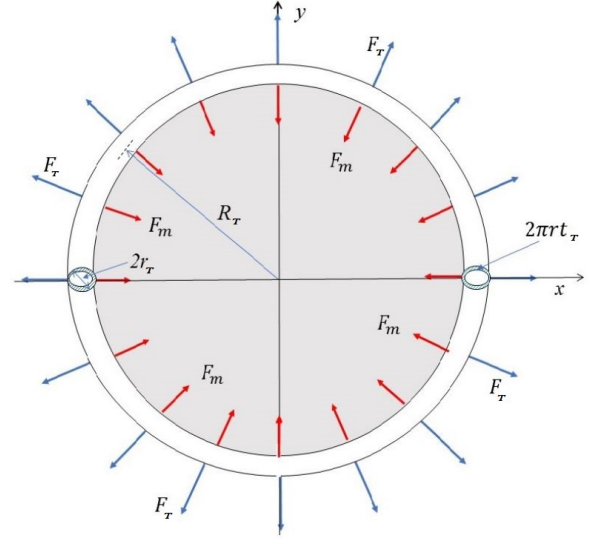

Fig. 6. Force on toroid

chosen to reduce the amount of variables and complexity. The key parameters of carbon fiber - epoxy matrix composite used for this thesis are

- Young's modulus, E_m, 70 GPa
- Ultimate strength, σ_u, 600 MPa
- Density, ρ_T, 1600 kg/m^3
- Poisson's ratio, υ, 0.1.

A beam subjected to bending will most often fail in three different modes, Euler buckling, local buckling and material collapse such as delamination yield or cracking. Furthermore, thin walled cylinders are especially sensitive to surface defects and thickness variation. A study found that a 20% variation of wall thickness may reduce the critical buckling load by half [29]. With this in mind, NASA developed a series of knockdown factors dependent on the type of load a thin walled structure cylindrical is subjected to. For the case of a thing walled cylinder under bending, the knockdown factor is expressed as

$$\gamma = 1 - 0.731(1 - e^{-\phi}) \tag{27}$$

where

$$\phi = \frac{1}{16\sqrt{t_T}}. \tag{28}$$

For the toroid, it is decided to assume a thickness-to-diameter ratio of 125. This is chosen due to the large amount of data [28] suggesting that this is a good middle ground for Euler and local buckling which are related to the length and thickness respectively. With a ratio set, a knockdown factor of 0.63 is calculated. For the handling analysis, several toroidal diameters are tested ranging from 10 to 100 mm, whilst keeping the 8 m diameter constant. Any toroids smaller than 10 mm diameter and 0.08 mm thick are deemed unfeasible due to the limit on available composite thicknesses. NASA points out that the knockdown factor may be conservative, but due

to the variable nature of composites, more advanced analysis should be done [30]. For this simple analysis, the knockdown factor and a basic approach reliant on solid mechanics was taken.

The cross sectional area and volume of the toroid are expressed as

$$A_T = \pi \left((d_T + t_T)^2 - d_T^2 \right), \qquad V_T = 2\pi R_t A_T \qquad (29)$$

where d_T is the inner diameter, and t_T is the thickness of the toroid. The force due to the mass F_T of the toroid is easily obtained by multiplying the volume by the material density ρ_T and the acceleration due to gravity:

$$F_T = \rho_T V_T g \qquad (30)$$

Considering the force acting on each of the cantilevered toroid halves is the mass of the toroid F_T, as well as the mass of the membrane F_m on one half of the toroid:

$$F_{\text{cg}_T} = \frac{F_T + (2F_m)}{2}. \qquad (31)$$

The bending moment $M_{\text{T base}}$ at the base, due to the force at the center of gravity, is:

$$M_{\text{T base}} = F_{\text{cg}_T} L_{\text{cg}} \qquad (32)$$

with L_{cg} being the distance from the base to the center of gravity.

The second moment of area I for the cross-section is given by:

$$I_t = \frac{\pi}{64} d_t^4. \qquad (33)$$

Thus, the bending stress σ_T experienced by the material is:

$$\sigma = \frac{M_{\text{T base}} r_T}{I}. \qquad (34)$$

Lastly, the maximum deflection $\delta_{\max_T}$ at the end of the cantilever is determined using

$$\delta_{\max} = \frac{F_{\text{cg}} R_T^3}{3EI}. \qquad (35)$$

E. Loads

To optimize the structure with respect to mass, a solid understanding of the loads it experiences throughout its life cycle is needed. The basis of this analysis and its justification is based off of two documents, ESA's *ECSS-E-HB-32-26A* [31] and NASA's *NASA-STD-5002A* [32] . They use "well proven methods, procedures and guidelines for the prediction and assessment of structural design loads and for the evaluation of the test loads". ESA defines the flight environments as either static (and quasi-static) or dynamic. The static or quasi-static loads (QSL) are defined as when the dynamic load has no significance on the structure. Typical dynamic loads can be seen in Tab. II. Due to the early stage of development and the complexity of dynamic structure response, only the static and quasi-static load analysis will be investigated without specifically looking at the dynamic influence.

TABLE II
SUMMARY OF SPACECRAFT LOAD TYPES AND THEIR TYPICAL FREQUENCIES

Load Type	Typical Frequency
LF Dynamic Response	Response from transient events 0-150 Hz
HF Random Vibration	From launch vehicle or transportation 20-2000 Hz
HF Acoustic Pressure	Dynamic load from payload compartment 20-8000 Hz
Shock Events	Sudden events triggering shock wave 500 Hz - 10 kHz

In essence, a quasi-static load combines both static and dynamic forces into a single static load used for design objectives. Designers often represent these loads as if they were static, typically converting them into an equivalent acceleration at the center of gravity, or "CoG net accelerations." These accelerations generally represent the extreme values—both maximum and minimum—that the center of gravity may experience. Quasi-static loads are closely linked to the conservative estimate of the most severe combinations of accelerations that can be encountered at any instant of the mission. This method has some limitations as outlined in the ESA report [31], but as they are conservative in terms of transient and static loads they still err on the side of caution in most cases. The load regimes identified are:

- Assembly and testing
- Transportation and handling
- Lift off and accent
- In situ.

During the assembly and testing phase, as well as all other Earth based phases, a gravitational force of **+1 G** acts on the structure. In addition to this, handling operations such as using a dolly or forklift may impart up to **+2 G** of vertical acceleration [32]. NASA did a large study in the early 70s in regards to transportation forces and found that land based transportation such as rail and road depended largely on foundation quality. Typically these forces do not exceed +3, −1 G. Air and water travel does not exceed +3, −1 and +2.25, −0.25 respectively [33]. Therefore, we can conclude that during the transportation phase the maximum acceleration is **+3 G**. The launch environment is the most extreme environment and also the most unpredictable due to the dynamic loads. For this thesis Spacex Falcon 9 and Arianespace Ariane 5 was investigated. These were chosen due to the wealth of data available in contrast with other launch vehicles as well as being the most common US and European launch vehicles in 2023. According to the Spacex user guide [34] an acceleration of 4 G is achieved during launch (no indication on if this is QSL, no other information could be found). The Ariane 5 cites a maximum quasi-static load of **+4.4 G** [35]. The in orbit acceleration from the solar pressure is difficult to calculate at this stage as the mass needs to be known, as seen in Eq. (8). However, by just estimating a mass and plugging it in it can be seen that the acceleration is of course extremely small. In the order of 10^{-6} G. In respect to structural failure, the in space environment will not be a limiting factor.

TABLE III
LOAD MAGNITUDE AND ITS REGIME

Source	Acceleration (G)
Gravity	1
On ground handling	2
Transportation	3.0
Launch	4.4
In situ	10^{-6}

3D Surface of Revolution around W_p axis
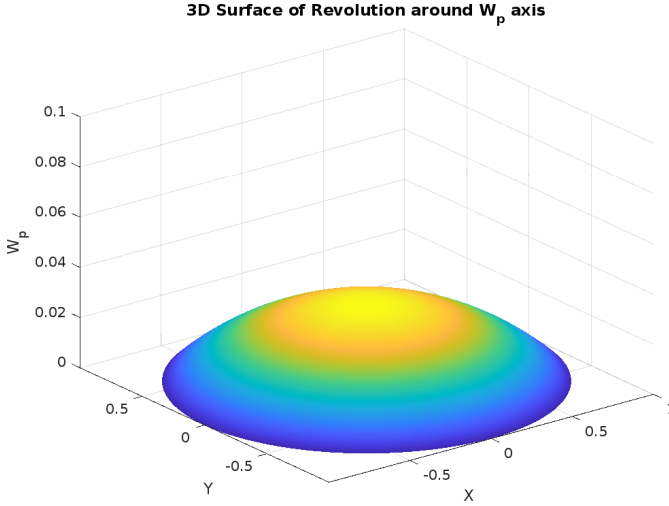

Fig. 7.   Membrane shape at 1 G

Fig. 8.   Displacement due to load regimes

IV. RESULT

A. Membrane

Using the method outlined in III-A a MATLAB code was created and implemented to solve the modified Hencky's problem presented. The three dimensional shape produced by the sagging membrane at maximum acceleration is seen in Fig. 7. However, it is of importance to note the normalised scale on the X-Y and Z axis. Moreover, Figs. 8 and 9 shows the displacement and stress across all the analyzed load regimes respectively. From these figures and Tab. V it is possible to analyse the proposed deflection limitation as well as stress limitations and an approximate safety factor in regards to the yield stress. The results show that according to the limitation of a 2% maximum deflection allowance, only the in situ and sag due to gravity is acceptable. Thus, according to the defined specifications, all types of sail handling and launch would require some type of support for the membrane.

TABLE IV
LOAD MAGNITUDE, ITS REGIME AND THE RESULTANT MEMBRANE
DISPLACEMENT

Source	Acceleration (G)	Max displacement (m)	Percentage of diameter
Gravity	1	0.147	1.8%
On ground handling	2	0.185	2.3 %
Transportation	3.0	0.212	2.6%
Launch	4.4	0.241	3.0%
In situ	10^{-6}	0.007	0%

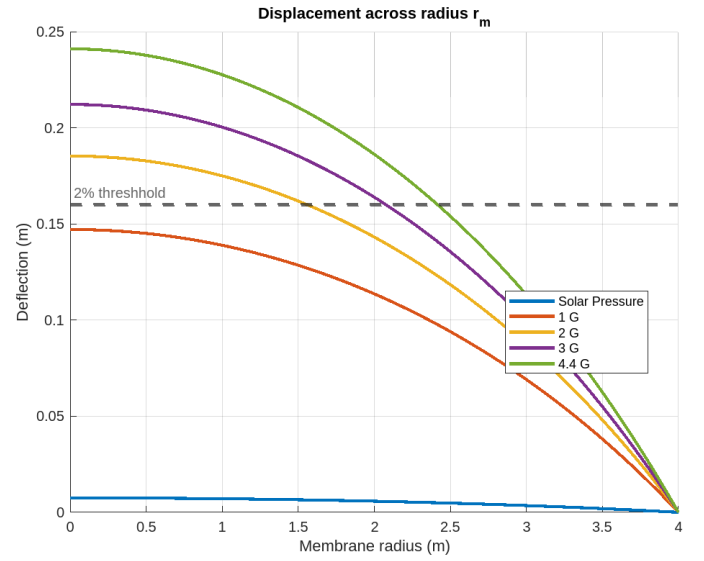In regards to the stress on the membrane, the maximum stress is located at the center of the membrane for all load cases, with a slight reduction closer towards the perimeter. As for the displacement, the stress on the membrane in orbit is vastly smaller than during the phases on Earth, on the order of 100 compared to during launch. Stress due to gravity, handling and transportation ranges from 19.6% to 30.7% of the yield stress. With safety factors at a minimum of 3.25, coupled with low dynamic forces, it is therefore concluded that the membrane will comply without failure during all handling and transportation phases on Earth. The launch environment, according to numbers from the launch providers, show a stress of 45.8 MPa, or 52.7%, giving a safety factor of 1.89. Whilst this may present itself like quite a large margin, one must take into account that this is due to a quasi-static load. The resultant forces from vibration and sound, especially on a large, thin, membrane structure such as our sail may induce heavy oscillations under the right circumstances. Based on these factors and unknowns, it is inconclusive if the sail would survive the launch environment due to the high stress loads in its current configuration. Further dynamic analysis is therefore needed to make correct judgments on the matter.

TABLE V
LOAD MAGNITUDE, THE RESULTANT STRESS AND PERCENTAGE OF YIELD
STRENGTH

Acceleration (G)	Maximum Stress (MPa)	Percentage of σ_y
1	17.07	19.6 %
2	27.09	31.1 %
3.0	35.45	30.7 %
4.4	45.83	52.7 %
10^{-6}	0.044	0.5 %

B. Bending of cantilever toroid

The particular situation of lifting the toroid on two opposing sides was modeled in MATLAB following the method previously outlined. The output is the mass, bending moment, bending stress and max deflection of the carbon fiber composite toroid, as a function of diameter and thickness. The
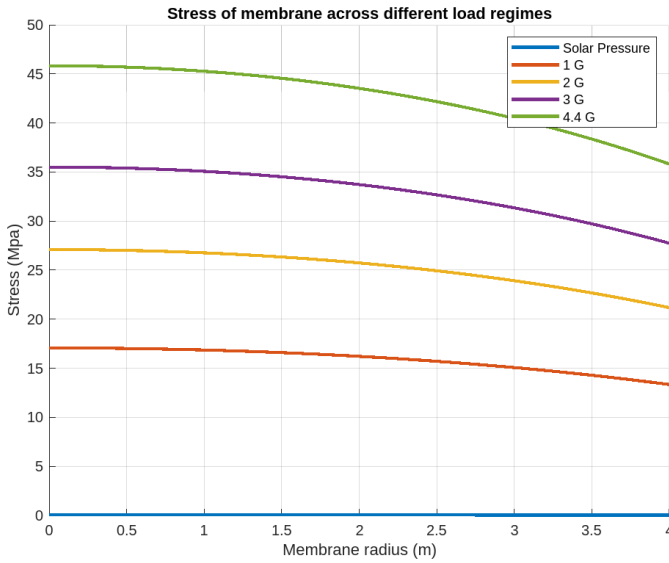
Fig. 9. Stress on membrane during different load regimes

Fig. 10. Bending of toroid under 1 G

results of this can be seen in Tab. VI. Furthermore, the bending stress of the toroid is graphed as a function of the tested diameters in Fig. 10. The bending stress was chosen as the determining factor for obvious reasons. As seen in the graph, the curve is exponentially decreasing as the diameter and wall thickness increases. In the method, it was assumed that the typical carbon fiber composite had an ultimate strength of 600 MPa. Moreover, a knockdown factor due to buckling for this particular load case was found to be 0.63. By combining, our final allowable stress is 378 MPa.

TABLE VI
STRUCTURAL ANALYSIS OF BENDING

Diameter (mm)	Thickness (mm)	mass (N)	Bending Moment (Nm)	Bending Stress (MPa)	Max Deflection (m)
10.00	0.08	0.99	6.43	654.8	1.40
20.00	0.16	3.97	10.67	135.8	0.15
30.00	0.24	8.92	17.73	66.9	0.05
40.00	0.32	15.86	27.62	44.0	0.02
50.00	0.40	24.79	40.34	32.9	0.01
60.00	0.48	35.69	55.88	26.3	0.01
80.00	0.64	63.45	95.44	19.0	0.01
100.00	0.80	99.14	146.30	14.9	0.00

C. Toroid

The buckling of the toroid ring based on Weeks [26] analytical investigation was modified and applied to the toroidal ring structure. In relation to how the load is applied during buckling, Weeks concluded that "The magnitude of the buckling load is very sensitive to the direction of loading during the buckling deformations". It was assumed that the load remains in the same direction under buckling. The toroidal-membrane interaction was thought to most closely mimic this scenario among the ones presented. Together with material data and chosen test geometries, a program was written to find the critical buckling loads. The results of which can be seen in Fig. 11. Moreover, the loads from the membrane is
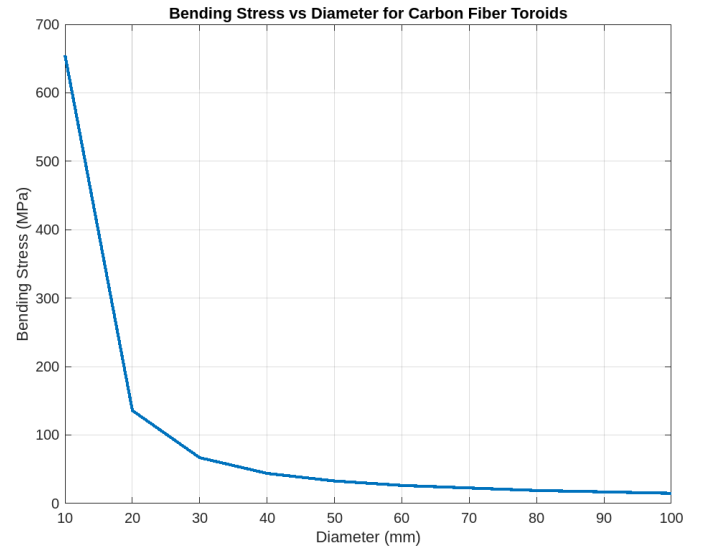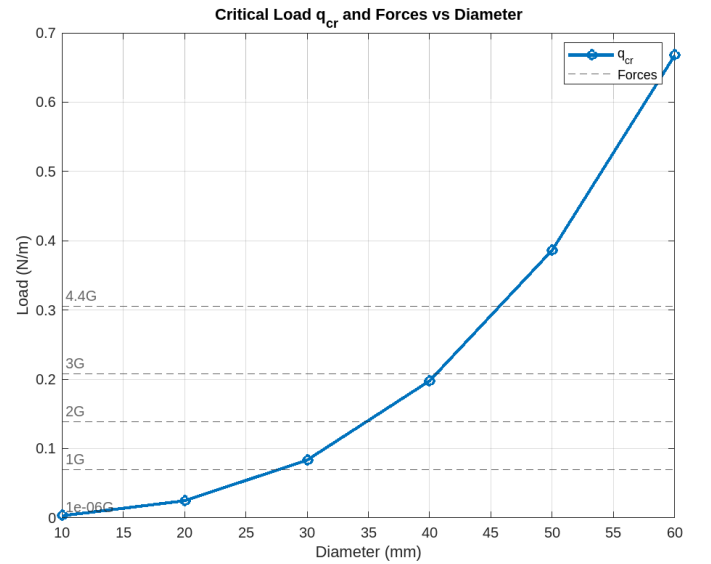

Fig. 11. Critical load and as a function of diameter

projected onto the toroid to find the load intensity due to the different accelerations, which can also be seen in Fig. 11 and Tab. VIII. It can be seen that q_{cr} increased quickly with larger diameters and thicker shell. At a diameter of 30 mm the toroid will support itself and the membrane under the gravitational conditions on Earth. This should be seen as a bare minimum for the structure and a trade off between this and larger diameters will be presented in the discussion.

V. DISCUSSION

From the results section, a multitude of data has been gathered and presented. In regards to membrane deflection a 2% maximum membrane deflection was proposed in the methods section. It was estimated that at this point material stress would start being a limiting factor as well. As seen from Fig 8, around 3% deflection is when the stress becomes the limiting factor. As for the stress, the membrane would have a

TABLE VII
STRUCTURAL BUCKLING OF TOROID

Diameter (mm)	Thickness (mm)	Mass (N)	Load Intensity (N/m)
10.00	0.08	0.99	0.003
20.00	0.16	3.97	0.025
30.00	0.24	8.92	0.084
40.00	0.32	15.86	0.198
50.00	0.40	24.79	0.387
60.00	0.48	35.69	0.67

TABLE VIII
LOAD INTENSITY q AT DIFFERENT ACCELERATIONS

Acceleration (G)	Load intensity (N/m)
1	0.070
2	0.139
3.0	0.208
4.4	0.306
10^{-6}	0

safety factor of 1.89 at launch according to our model. It was mentioned in the section that despite 1.89 seeming adequate, this may not be the case. This is due to the non-ideal geometry of the membrane. The membrane, when properly attached to the toroid, will act like a drum, amplify any vibrations and oscillate rapidly. The quasi-static load expressed by ESA covered static and transient loads, but due to their chaotic nature, forces such as sound and other vibrations was not properly taken into account. While the 1.89 safety factor may comply with the launch environment, it cannot be concluded at this point. More modeling and testing needs to be conducted and may come to the conclusion that a support is needed. Furthermore, it may be beneficial to have some membrane support structure throughout the journey of the sail, until launch, as the excessive sagging may be problematic.

The lifting and subsequent bending of the toroid during handling, for example, has been dealt with. In this specific case, it was investigated if the structural mass of the toroid and membrane would snap the carbon fiber toroid when lifted at two opposite points. Referencing Tab. VI, it is seen that the 20 mm toroid is the first iteration to fall under the limit of 378 MPa, giving a safety factor of 2.78. The maximum deflection at the tips are at 15 cm and deemed to be reasonable given the 8 meter diameter. This however, only applies in this specific circumstance, and should not be seen as the final toroid size.

The buckling of the carbon fiber toroid structure during different phases of the life cycle produced a critical buckling load for several tested diameters and thicknesses. As expected, the load which the structure can sustain increases quickly as the diameter and thickness increases. This is due to the large influence on moment of inertia from the diameter increase and the thicker shell being more resilient to local buckling. The primary drawbacks of which are, in combination with the volume increase, the mass. Therefore, it is a more complex optimization problem which requires careful consideration. While it may seem straightforward to choose the first size that satisfies the launch environment, i.e. 50 mm in this case, a more overarching approach may be taken.

As stated in the introduction minimizing mass is of the utmost importance for solar sail performance. A different, potentially beneficial, approach could therefore be to size the toroid to survive the Earth environment at 1 G and some light lifting, which is a maximum of 1.5 G. The structure could be produced, assembled and subsequently put on a supporting structure necessary for transport and launch. This structure would separate in orbit leaving the mass optimised sail in the low acceleration environment by itself. This approach may be more costly mass wise to bring into orbit, but may greatly increase spacecraft performance. For example, if the toroid needs to support 1.5 G, with some margin, a diameter of 35 mm would suffice. In contrast to the 50 mm needed to survive launch, the 35 mm toroid weighs 1.24 kg compared to 2.53 kg. A 50% decrease in final toroid mass, and a lower lightness number for the sail. There are of course negatives associated with adding jettisonable support structure in addition to the mass. These include move volume and more complexity and sources of error in the spacecraft design.

VI. CONCLUSION

A brief overview and history of solar sails has been presented. The problem of a mass optimized circular solar sail has been investigated through several different aspects and during its life cycle. These include stress and strain on the membrane and the buckling of a carbon fiber toroid structure. The thesis has taken a solid mechanics approach to solving these problems. It was found that state of the art membrane material may stand up to the stress of all phases during its time on Earth and in orbit. But it may benefit from support limiting deformation. A minimum diameter and thickness was found to support lifting of the toroids middle, although this was lower than the proposed final proposed diameter of 35 mm. Finally, it was argued that rather than sizing the toroid strength to survive the launch, it may be beneficial to add a jettisonable structure to minimize mass and therefore produce a higher lightness number and have better overall performance. This thesis has tried to err on the side of caution as many times cutting edge technologies such as material data and performance figures maybe presented over-optimistically. As with all spaceflight, it is a complex issue which requires extensive resources and research. However, the application of multiple low cost, low mass, circular solar sails connected together to tow a payload seems like one of the more viable uses for solar sails.

VII. FUTURE WORK

In general, solar sails receive quite little attention in comparison with traditional propulsion methods due to their narrow applicability. As material science progresses solar sailing will become more viable. Much future development needs to be done on the more practical and plausible use cases for solar sails and shades. At the moment, the gap between viable missions and academic proposals need to be bridged. For this thesis, an approach centered around solid mechanics was taken. To increase trustworthiness in the quantitative data put forth, FEM analysis would be of great benefit. Furthermore, the strength of the structures touched upon in this thesis are very geometry dependant. Whilst empirical data exist for

related structures none such exist in this case. Equations from these test have been extrapolated and used in this thesis which may be inaccurate, but cannot be determined without empirical testing at this time.

REFERENCES

[1] C. Fuglesang and M. G. de Herreros Miciano, "Realistic sunshade system at l1 for global temperature control," *Acta Astronautica*, vol. 186, pp. 269–279, 2021. [Online]. Available: https://www.sciencedirect.com/science/article/pii/S0094576521001995

[2] D. Miller, F. Duvigneaud, W. Menken, D. Landau, and R. Linares, "High-performance solar sails for interstellar object rendezvous," *Acta astronautica*, vol. 200, pp. 242–252, 2022.

[3] M. Ceriotti, C. McInnes, and B. Diedrich, "The pole-sitter mission concept: An overview of recent developments and possible future applications," vol. 3, 01 2011, pp. 2543–2559.

[4] C. A. Bailer-Jones, "The sun diver: Combining solar sails with the oberth effect," *American Journal of Physics*, 2020, accepted on 26 September 2020.

[5] J. Heiligers, B. Diedrich, W. Derbes, and C. McInnes, "Sunjammer: Preliminary end-to-end mission design," 08 2014.

[6] T. Ingrassia, V. Faccin, A. Bolle, C. Circi, and S. Sgubini, "Solar sail elastic displacement effects on interplanetary trajectories," *Acta astronautica*, vol. 82, pp. 263–272, 2013.

[7] Z. Pengyuan, W. Chenchen, and L. Yangmin, "Design and application of solar sailing: A review on key technologies," *Chinese Journal of Aeronautics*, vol. 36, no. 5, pp. 125–144, 2023. [Online]. Available: https://www.sciencedirect.com/science/article/pii/S1000936122002564

[8] G. Greschik and E. Montgomery, "Space tow solar sails: Design study exploring performance and operational issues," 04 2007.

[9] A. Finkbeiner, "Inside the breakthrough starshot mission to alpha centauri," Dec. 2016, 18 min read.

[10] D. L. Edwards, W. A. Hollermad, W. S. Hubbs, P. A. Gray, G. E. Wed, D. T. H ppe, M. K. Nehls, and C. L. Semmel, "Electron radiation effects on candidate solar sail material."

[11] E. Flores Garcia, "Simulation of attitude and orbital disturbances acting on aspect satellite in the vicinity of the binary asteroid didymos," School of Electrical Engineering, 2016, thesis submitted for examination for the degree of Master of Science in Technology. Espoo December 6, 2016.

[12] R. Miller, "Solar sails."

[13] NASA, "NASA's Nanosail-D 'Sails' Home – Mission Complete," https://www.nasa.gov, 2011, archived from the original on 2011-12-01. Retrieved 2012-01-04.

[14] V. Y. Kezerashvili and R. Y. Kezerashvili, "Solar sail with superconducting circular current-carrying wire," *Advances in Space Research*, vol. 69, no. 1, pp. 664–676, 2022.

[15] J. L. Wright, *Space Sailing*, illustrated ed. Taylor & Francis, 1992.

[16] G. Greschik, A. Palisoc, and M. M. Mikulas, "Revisiting hencky's problem — approximations in the power series solution," *Center for Aerospace Structures, University of Colorado*, 2003, iGarde, Inc., Tustin, CA.

[17] X. Li, J.-Y. Sun, Z.-H. Zhao, S.-Z. Li, and X.-T. He, "A new solution to well-known hencky problem: Improvement of in-plane equilibrium equation," *Mathematics*, vol. 8, p. 653, 04 2020.

[18] H. Hencky, "On the stress state in circular plates with vanishing bending stiffness," *Zeitschrift für Mathematik und Physik*, vol. 63, pp. 311–317, 1915.

[19] W. B. Fichter, "Some solutions for the large deflections of uniformly loaded circular membranes," *NASA Technical Paper 3658*, 1997.

[20] R. Y. Kezerashvili, "Thickness requirement for solar sail foils," *Acta Astronautica*, vol. 65, pp. 507–518, 2009, received 31 July 2008. [Online]. Available: http://www.elsevier.com/locate/actaastro

[21] W. K. Wilkie, J. M. Fernandez, O. R. Stohlman, N. R. Schneider, G. D. Dean, J. H. Kang, J. E. Warren, S. M. Cook, J. Heiligers, and Others, "Overview of the nasa advanced composite," in *AIAA Scitech 2021 Forum*, vol. 1 PartF. American Institute of Aeronautics and Astronautics Inc. (AIAA), 2021, pp. 1–23, aIAA 2021-1260.

[22] O. R. Stohlman, J. M. Fernandez, G. D. Dean, N. Schneider, J. H. Kang, R. Barfield, T. Herndon, and P. Stokes, "Advances in low-cost manufacturing and folding of solar sail membranes."

[23] K. Jin Ho, K. Gordon, R. Bryant, R. S. Olive, and W. Keats, "Durability characterization of mechanical interfaces in solar sail membrane structures," *Advances in Space Research*, vol. 67, no. 9, pp. 2643–2654, 2021, solar Sailing: Concepts, Technology, and Missions II. [Online]. Available: https://www.sciencedirect.com/science/article/pii/S0273117720305731

[24] O. Stohlman, J. Fernandez, G. Dean, N. Schneider, J. Kang, R. Barfield, T. Herndon, and P. Stokes, "Advances in low-cost manufacturing and folding of solar sail membranes," 01 2020.

[25] I. Senjanovic, D. Čakmak, N. Alujević, I. Ćatipović, and N. Vladimir, "Ring buckling analysis based on the toroidal shell theory," *Transactions of FAMENA*, vol. 44, pp. 1–12, 05 2020.

[26] G. E. Weeks, "Buckling of a pressurized toroidal ring under uniform external loading," *NASA TN D-4124*, 1967.

[27] E. Hedlund, "Surface accuracy analysis of axisymmetric inflatable reflector antennas," Master's Thesis, Royal Institute of Technology, Department of Mechanics, SE-100 44 Stockholm, Sweden, June 2006.

[28] X. Hui, Z. Lei, Z. Bing, Y. Houfeng, L. Debao, W. Huabi, and Z. Bin, "Static and dynamic bending behaviors of carbon fiber reinforced composite cantilever cylinders," *Composite Structures*, vol. 201, pp. 893–901, 2018. [Online]. Available: https://www.sciencedirect.com/science/article/pii/S0263822318317458

[29] P. Weaver, "Design of laminated composite cylindrical shells under axial compression," *Composites Part B: Engineering*, vol. 31, no. 8, pp. 669–679, 2000. [Online]. Available: https://www.sciencedirect.com/science/article/pii/S1359836800000299

[30] National Aeronautics and Space Administration, "Buckling of thin-walled circular cylinders," NASA, NASA SP 8007, 8 1968, originally published in September 1965, Revised in August 1968.

[31] *Spacecraft Mechanical Loads Analysis Handbook*, Ecss-e-hb-32-26a ed., European Space Agency, ESTEC, P.O. Box 299, 2200 AG Noordwijk, The Netherlands, 2 2013, published by ESA Requirements and Standards Division. Significant contributions by A. Calvi.

[32] J. Roe, Ralph R., "Load analyses of spacecraft and payloads," Office of the NASA Chief Engineer, NASA Technical Standard NASA-STD-5002A, 9 2019, approved: 2019-09-25, Superseding NASA-STD-5002. [Online]. Available: https://standards.nasa.gov/sites/default/files/standards/NASA/A/0/nasa-std-5002a.pdf

[33] National Aeronautics and Space Administration, "Space vehicle design criteria (structures): Transportation and handling loads," NASA, NASA Space Vehicle Design Criteria SP-8077, 9 1971. [Online]. Available: https://ntrs.nasa.gov/api/citations/19720005242/downloads/19720005242.pdf

[34] *Falcon 9 User's Guide*, SpaceX, 9 2021. [Online]. Available: https://www.spacex.com/media/falcon-users-guide-2021-09.pdf

[35] E. Perez, *Ariane 5 User's Manual*, issue 5 revision 1 ed., Arianespace, 7 2011. [Online]. Available: https://www.arianespace.com/wp-content/uploads/2015/09/Ariane5_users_manual_Issue5_July2011.pdf